Calculation of Three-Dimensional Flowfields by the Unsteady Method of Characteristics

David L. Marcum* and Joe D. Hoffman†
Purdue University, West Lafayette, Indiana

A numerical algorithm based on the unsteady three-dimensional method of characteristics is presented for calculating unsteady three-dimensional subsonic/transonic inviscid flowfields. The flowfield unit processes are based on a local network consisting of six bicharacteristics and the pathline. The algorithm is an explicit second-order accurate predictor-corrector procedure. An inverse-marching method is employed, wherein the solution grid in physical space is prespecified. Steady flow solutions are obtained as the asymptotic solution in time. Results are presented for spherical supersonic source flow, for axisymmetric supersonic flow in a conical nozzle, for three-dimensional supersonic flow in a superelliptical nozzle, and for three-dimensional subsonic/transonic flow in a superelliptical nozzle. Solutions obtained by the present method agree well with solutions obtained by steady flow method of characteristics algorithms and experimental data.

Nomenclature

a = speed of sound
$\bar{n}$ = characteristic surface physical unit normal (n_x, n_r, n_θ)
P = pressure
t = time
u, v, w = velocity components
x, r, θ = cylindrical coordinates
ρ = density

Introduction

THE objective of this investigation was to develop a numerical method of characteristics algorithm for calculating unsteady three-dimensional inviscid flowfields. The algorithm can be used to solve both unsteady and steady flowfields as the asymptotic solution in time.

The numerical procedure is based on the bicharacteristic method proposed by Butler.[1] Butler's method is based on a local network of bicharacteristics and the pathline. The method is an explicit second-order accurate predictor-corrector procedure. Butler's method has been applied to steady three-dimensional flow problems by Ransom et al.,[2] Cline and Hoffman,[3] and Vadyak et al.[4] Delaney and Kavanagh[5] and Shin and Valentin[6] have applied Butler's method to unsteady two-dimensional flow problems. In the present investigation,[7] Butler's method is extended to unsteady three-dimensional flow. Several nozzle flowfields are computed to demonstrate the capabilities of the method.

Approach

Essentially, the method of characteristics is a coordinate transformation in which the computational coordinates (i.e., the characteristic surfaces) are also the paths of propagation of information in the physical space. This close matching of the numerical and physical propagation paths results in an extremely accurate modeling of the flowfield. Fixed-grid finite difference methods, which propagate information along coordinate lines instead of the physical propagation paths, do not model the physics of the flow as well as the method of characteristics. To date, there has been no application of the method of characteristics to a complete unsteady three-dimensional flow problem. However, the numerical procedure has been developed by Hoffman.[8]

The advantage of the method of characteristics over fixed-grid finite difference methods, such as MacCormack's method,[9] is obvious. So why is it not used more frequently? There are three major reasons.

1) It is a relatively complicated procedure, especially in three or four independent variables.

2) The method is restricted to flows without discontinuities (e.g., shock waves and contact surfaces).

3) Due to its complexity, computer codes based on the method of characteristics typically require more execution time.

Admittedly, these are formidable disadvantages. However, they can all be surmounted with patience, devotion, and tender loving care.

The first disadvantage, the complexity of the method of characteristics in three or four variables, is overcome simply by devoting sufficient effort to understand the method. Hoffman[8] presents a detailed discussion of the method for unsteady one-, two-, and three-dimensional flows. The books by Zucrow and Hoffman[10] present detailed discussions and applications of the method to two- and three-variable problems.

The second disadvantage, the restriction to continuous flows, is a more serious limitation. In supersonic flowfields with a limited number of discrete shock waves, the shock waves can be discretely fitted and the method of characteristics can be employed between the shock waves. In subsonic flows, shock waves do not exist. In transonic flows, shock waves, if they do exist, are quite weak, and can be smeared by the method of characteristics.

The third disadvantage, the longer execution times of programs based on the method of characteristics as compared to programs based on fixed-grid finite difference methods, can be minimized by careful development of the numerical algorithm. The longer execution times are caused mainly by the following three procedures: 1) construction of the network of characteristic surfaces, 2) iteration of the modified-Euler corrector, and 3) interpolation for flow properties in the initial-value surface.

Presented as Paper 84-0440 at the AIAA 22nd Aerospace Sciences Meeting, Reno, Nev., Jan. 9-12, 1984; received March 4, 1984; revision received Nov. 29, 1984.

*Research Assistant, Mechanical Engineering, Thermal Sciences and Propulsion Center. Student Member AIAA.

†Professor, Mechanical Engineering, Thermal Sciences and Propulsion Center. Member AIAA.

The additional effort required to construct the characteristic network cannot be completely avoided, but can be minimized by employing an inverse method wherein the solution points are prespecified on a regular grid and a local characteristic network is constructed. The numerical procedure developed by Butler[1] is based on a local network of bicharacteristic lines (i.e., lines tangent to characteristic surfaces that are analogous to Mach lines in steady two-dimensional supersonic flow) and pathlines. The construction of these lines is very simple, thus minimizing the work required to construct the characteristic network.

The time required to iterate the modified-Euler corrector can be completely eliminated by simply eliminating the iterative steps in the procedure. The resulting algorithm is still second-order accurate.

The third major time consumer, which is present in any inverse-marching method, is the large amount of interpolation required in the initial-value surface to obtain the flow properties at the points of intersection of the rearward-projected bicharacteristics and pathline from the prespecified solution points with the initial-value surface. There is no way to eliminate the requirement of interpolation in an inverse method, but the work required can be minimized by careful planning. Typically quadratic least-squares polynomials are fit to the data in the initial-value surface. Those polynomials are then evaluated at the points of intersection of the bicharacteristics and the pathline with the initial-value surface to determine the flow properties. Heretofore, all bicharacteristic methods have used some form of nonuniform grid in the physical space. Thus, fitting the least-squares polynomials must be done over and over at all grid points at each time step. By working in a body-fitted uniform computational grid, the least-squares polynomials can be determined once for all grid points for all time. This procedure alone has the potential to halve the computational time of programs based on the method of characteristics.

The method of characteristics algorithm developed in the present investigation has been optimized to achieve maximum efficiency without sacrificing accuracy. The numerical procedure is very straightforward to implement on both scalar and vector processors. The execution time is comparable to that for fixed-grid finite difference algorithms.

Gas Dynamic Model

The gas dynamic model is based on the following assumptions: 1) unsteady three-dimensional flow, 2) inviscid nonconducting fluid with no body forces, and 3) a simple system in thermodynamic equilibrium. The governing equations consist of the continuity equation, the component momentum equations, the energy equation, and the thermal and caloric equations of state. A cylindrical coordinate system was employed in the analysis. The velocity components in the x, r, and θ directions are denoted by u, v, and w, respectively. The governing equations are

$$\rho u_x + \rho v_r + \rho w_\theta/r + u\rho_x + v\rho_r + w\rho_\theta/r + \rho_t = -\rho v/r \quad (1)$$

$$\rho u u_x + \rho v u_r + \rho w u_\theta/r + \rho u_t + P_x = 0 \quad (2)$$

$$\rho u v_x + \rho v v_r + \rho w v_\theta/r + \rho v_t + P_r = \rho w^2/r \quad (3)$$

$$\rho u w_x + \rho v w_r + \rho w w_\theta/r + \rho w_t + P_\theta/r = -\rho v w/r \quad (4)$$

$$uP_x + vP_r + wP_\theta/r + P_t - a^2(u\rho_x + v\rho_r + w\rho_\theta/r + \rho_t) = 0 \quad (5)$$

The thermal equation of state and the speed of sound are specified by the functional relationships $T = T(P,\rho)$ and $a = a(P,\rho)$, respectively.

Method of Characteristics

Systems of quasilinear partial differential equations of first order in four independent variables (three space variables and time) have the property that there exist special hypersurfaces (called characteristic hypersurfaces) in four-dimensional hyperspace on which linear combinations of the original partial differential equations can be formed that contain derivatives only in the special hypersurfaces themselves. These linear combinations are interior operators called compatibility relations. A complete derivation of the characteristic equations and compatibility relations for unsteady three-dimensional flow is presented by Hoffman[8] and Rusanov.[11] A summary of those results, in the cylindrical coordinate system, is presented in this section.

For unsteady three-dimensional flow, two families of characteristic hypersurfaces exist. One family of characteristic hypersurfaces consists of stream hypersurfaces, which are hypersurfaces composed of pathlines. The envelope of all of the stream hypersurfaces passing through a point is the unique pathline passing through the point. A pathline is specified by

$$dx = u\,dt, \qquad dr = v\,dt, \qquad d\theta = (w/r)\,dt \quad (6)$$

The compatibility relations that are valid on a stream hypersurface are

$$\rho \bar{W}_i \cdot \frac{D\bar{V}}{Dt} + d_{\bar{W}_i} P = 0 \quad (7)$$

which is valid on three independent stream hypersurfaces, each containing an independent vector $\bar{W}_i$ $(i = 1,2,3)$ that lies entirely in physical space, and

$$\frac{DP}{Dt} - a^2 \frac{D\rho}{Dt} = 0 \quad (8)$$

which is applicable along the envelope of the stream hypersurfaces (i.e., the pathline). The notation D( ) denotes the total differential of ( ) along the pathline.

The other family of characteristic hypersurfaces consists of wave hypersurfaces. The envelope of all wave hypersurfaces at a point forms the Mach hyperconoid. The Mach hyperconoid of differential size is a right circular hypercone known as the Mach hypercone. The line of contact between a particular wave hypersurface and the Mach hyperconoid is known as a bicharacteristic. Thus, a bicharacteristic is a generator of the Mach hyperconoid.

Butler[1] proposed a parametric representation for a bicharacteristic and the wave hypersurface compatibility relation that is valid along a bicharacteristic. When applied to unsteady three-dimensional flow, that parametric representation is

$$dx = (u - an_x)\,dt, \quad dr = (v - an_r)\,dt, \quad d\theta = (w - an_\theta)\,dt/r \quad (9)$$

where n_x, n_r, and n_θ are the physical components of the unit normal vector $\bar{n}$ to the characteristic hypersurfaces. The compatibility relation valid along wave hypersurfaces is

$$\begin{aligned} &\frac{\mathfrak{D}P}{\mathfrak{D}t} - \rho a n_x \frac{\mathfrak{D}u}{\mathfrak{D}t} - \rho a n_r \frac{\mathfrak{D}v}{\mathfrak{D}t} - \rho a n_\theta \frac{\mathfrak{D}w}{\mathfrak{D}t} \\ &- \rho a^2 \left[(n_x^2 - 1)u_x + (n_r^2 - 1)v_r + \frac{(n_\theta^2 - 1)w_\theta}{r} \right. \\ &\left. + n_x n_r (u_r + v_x) + n_x n_\theta \left(\frac{u_\theta}{r} + w_x \right) + n_r n_\theta \left(\frac{v_\theta}{r} + w_r \right) \right] \\ &= -\frac{\rho a^2 v}{r} - \frac{n_r \rho a w^2}{r} + \frac{n_\theta \rho a v w}{r} \end{aligned} \quad (10)$$

where the notation $\mathfrak{D}(\ )$ denotes the total differential of ( ) along the bicharacteristic. The terms u_x, u_r, u_θ, v_x, etc., which are called cross derivatives, represent differentiation in the wave hypersurfaces in a direction normal to the bicharacteristic direction.

Two infinite families of characteristic hypersurfaces exist at each point in the flowfield: stream hypersurfaces and wave hypersurfaces. One compatibility relation applies along the envelope of the stream hypersurfaces (i.e., the pathline), one compatibility relation is valid on each of three independent stream hypersurfaces, and one compatibility relation applies on each wave hypersurface. Consequently, an infinite number of compatibility relations apply at each point in the flowfield. However, these compatibility relations are merely linear combinations of the original system of governing partial differential equations, Eqs. (1-5). Since there are five independent equations in that system, only five linear combinations of those five governing equations can be independent. Consequently, only five of the infinite number of compatibility relations are independent.

Rusanov[11] has shown that four independent sets of compatibility relations exist for unsteady three-dimensional flow. The following independent set is employed in the present study: Eq. (8) applied along the pathline and Eq. (10) applied along four independent bicharacteristics.

An inverse-marching method is employed to construct the finite difference grid. The grid points are prespecified on hypersurfaces of constant time. The time step between successive solution hypersurfaces is chosen to satisfy the Courant-Friedrichs-Lewy (CFL) stability criterion.[12] The pathline and bicharacteristics are projected rearward to the initial-data hypersurface (i.e., the $xr\theta$ hypersurface in the $xr\theta t$ hyperspace) to determine the initial-data points. The flow properties at the initial-data points are determined by fitting interpolating polynomials to the initial-data hypersurface. Least-squares quadratic trivariate interpolating polynomials are employed. The cross derivatives are found by differentiating the interpolating polynomials.

The characteristic equations and compatibility relations are integrated by the second-order accurate modified-Euler predictor-corrector numerical integration method. For the predictor, all coefficients, cross derivatives, and nonhomogeneous terms are evaluated at the initial-data points. For the corrector, all coefficients, cross derivatives, and nonhomogeneous terms are evaluated as averages between the initial-data points and the solution point. A problem arises with the evaluation of the cross derivatives at the solution point. The procedure of differentiating the interpolating polynomials cannot be employed in the solution hypersurface without using points adjacent to the solution point to determine the interpolating polynomials, which violates the domain of dependence of the solution point.

Butler[1] eliminated this problem for flows having three independent variables by devising an ingenious scheme that explicitly eliminates the cross derivatives at the solution point from the finite difference equations using a noncharacteristic relation. The noncharacteristic relation is a linear combination of the continuity and energy equations [Eqs. (1) and (5)] in which the derivatives of density are eliminated. Thus,

$$\frac{DP}{Dt} + \rho a^2 \nabla \cdot \bar{V} = 0 \tag{11}$$

Equation (11) may be applied along a pathline by considering DP/Dt as a directional derivative along the pathline and $\nabla \cdot \bar{V}$ as cross derivatives.

Butler's method is extended to unsteady three-dimensional flow by replacing the set of four independent bicharacteristic compatibility relations by a set of six bicharacteristic compatibility relations and the noncharacteristic relation, Eq. (11). Four linear combinations of the finite difference forms of those seven equations are formed, which explicitly eliminate the cross derivatives at the solution point. Those four equations and the finite difference form of the energy equation applied along the pathline comprise a set of five independent finite difference equations for determining the five flow properties u, v, w, P, and ρ.

Transformed Interpolating Space

In the overall numerical algorithm, an inverse-marching method is employed. The solution points in physical space are prespecified. In general, the physical grid is neither orthogonal nor uniform. A local characteristic network is constructed at each point by the rearward projection of bicharacteristics and the pathline. The nonuniform physical space is transformed to a uniform transformed space used

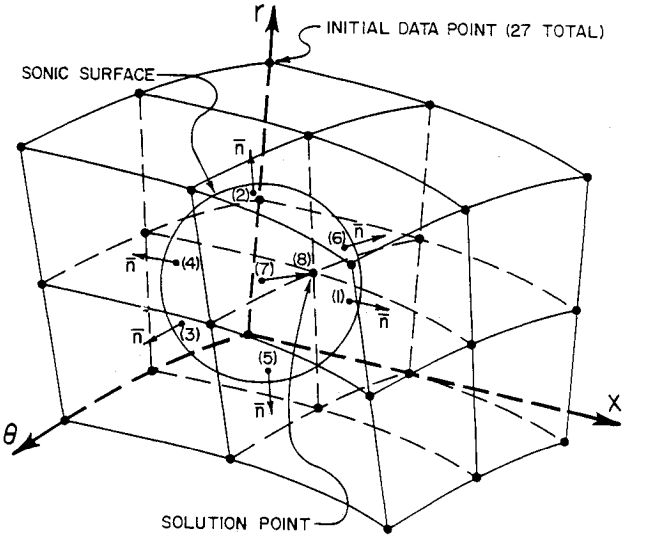

Fig. 1 Interior point unit process.

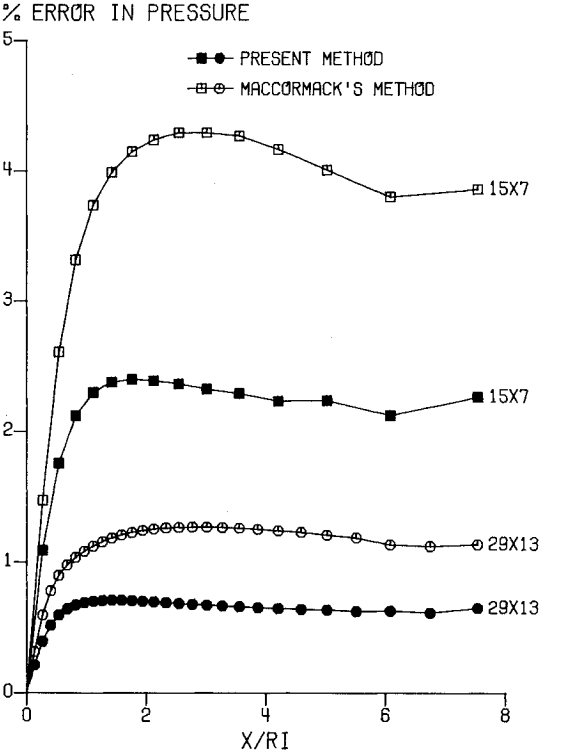

Fig. 2 Errors in wall static pressure.

only for interpolation. The compatibility relations are solved in the nonuniform physical space. The use of a transformed interpolating space is an essential feature of the present algorithm. The details of the interpolating procedure are presented by Marcum and Hoffman.[7]

Unit Processes

A variety of unit processes is employed in the computation of the flowfield. There are five basic types of flowfield points to be computed: interior, solid boundary, inlet, exit, and axis points. The basic features of the interior point unit process are presented in the following discussion. A brief description of the other four unit processes is presented.

Interior Point Unit Process

The projection of the finite difference grid for an interior point on the physical space $xr\theta$ is illustrated in Fig. 1. The location of the solution point, point 8, in physical space is prespecified. The volume enclosed by the eight initial-data points on the corners of the finite difference network comprises the domain of dependence of the finite difference equations (commonly called the convex hull), and the sonic surface created by the intersection of the rearward-projected Mach hyperconoid and the initial-data hypersurface comprises the domain of dependence of the partial differential equations.

The flow properties in the initial-data hypersurface are determined by a least-squares quadratic trivariate curve fit in the transformed interpolating space of the data at the 27 initial-data points in the finite difference grid.

Point 7 is the intersection point of the rearward-projected pathline from point 8 in the solution hypersurface with the initial-data hypersurface. For the overall predictor, u, v, and w are evaluated at point 8 in the initial-data hypersurface using the interpolating polynomials, and the finite difference form of Eq. (6) is then solved for the location of point 7. The flow properties at point 7 are then determined from the interpolating polynomials. The location of point 7 is not iterated during either the predictor or corrector of the overall algorithm. For the corrector, average values of u, v, and w between point 7 in the initial-value hypersurface and point 8 in the predictor solution hypersurface are employed.

Points 1-6 are the intersection points of six rearward-projected bicharacteristics from point 8 in the solution hypersurface with the initial-data hypersurface. Those points are determined from the finite difference forms of Eq. (9). Six bicharacteristics are required in the numerical integration scheme. The most convenient six are those corresponding to $\bar{n} = \pm\bar{i}_x$, $\pm\bar{i}_r$, and $\pm\bar{i}_\theta$ at the points of intersection of the bicharacteristics and the initial-data hypersurface. The procedure described above to solve Eq. (6) is employed to solve Eq. (9). The flow properties at points 1-6 are determined from the interpolating polynomials.

The flow properties at the solution point are determined by numerically integrating the compatibility relations along the generators of the finite difference grid. The bicharacteristic compatibility relation, Eq. (10), is applied along the six bicharacteristics. For example, the result along bicharacteristic 1-8 for the predictor is

$$P_8 - (\rho a)_1 u_8 = C_1 \tag{12}$$

$$C_1 = P_1 - (\rho a)_1 u_1 - \{(\rho a^2)_1 [v_r(1) + w_\theta(1)/r_1] + (\rho a^2 v/r)_1\}\Delta t \tag{13}$$

Similar equations are obtained along the other five bicharacteristics. The finite difference form of the noncharacteristic relation, Eq. (11), applied along the pathline is

$$P_8 = P_7 - \{(\rho a^2)_7 [u_x(7) + v_r(7) + w_\theta(7)/r_7] + (\rho a^2 v/r)_7\}\Delta t \tag{14}$$

A set of seven finite difference equations is obtained. This set is reduced to four independent equations by adding the bicharacteristic compatibility relations along bicharacteristics 1-8 and 4-8, 2-8 and 5-8, and 3-8 and 6-8. The pressure P_8 is obtained from Eq. (14), and the velocity components u_8, v_8, and w_8 are obtained from the three independent combinations of the bicharacteristic compatibility relations. The density ρ_8 is determined from the finite difference form of the energy equation, Eq. (8), applied along the pathline.

For the corrector, the cross derivatives at the solution point are explicitly eliminated from the finite difference equations. For example, the finite difference equations along bicharacteristics 1-8 and 4-8 are

$$P_8 - (\rho a)_{18} u_8 + \tfrac{1}{2}(\rho a^2)_8 [v_r(8) + w_\theta(8)/r_8]\Delta t = C_1 \tag{15}$$

$$C_1 = P_1 - (\rho a)_{18} u_1 - \{\tfrac{1}{2}(\rho a^2)_1 [v_r(1) + w_\theta(1)/r_1] + (\rho a^2 v/r)_{18}\}\Delta t \tag{16}$$

$$P_8 + (\rho a)_{48} u_8 + \tfrac{1}{2}(\rho a^2)_8 [v_r(8) + w_\theta(8)/r_8]\Delta t = C_4 \tag{17}$$

$$C_4 = P_4 + (\rho a)_{48} u_4 - \{\tfrac{1}{2}(\rho a^2)_4 [v_r(4) + w_\theta(4)/r_4] + (\rho a^2 v/r)_{48}\}\Delta t \tag{18}$$

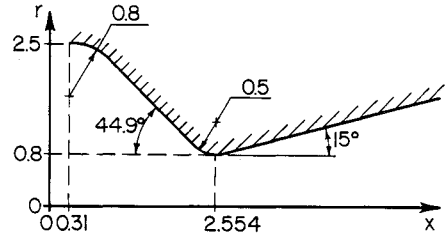

Fig. 3 Conical nozzle.

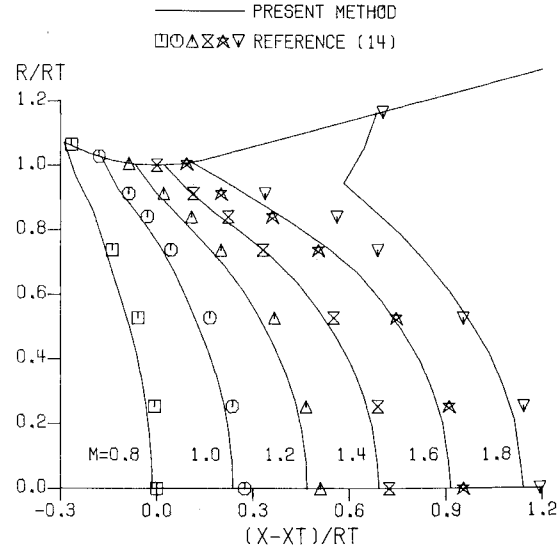

Fig. 4 Transonic Mach number contours.

where the double subscripts denote average values along the appropriate bicharacteristics. Subtracting Eq. (15) from Eq. (17) yields

$$[(\rho a)_{18} + (\rho a)_{48}]u_8 = (C_4 - C_1) \tag{19}$$

Similar results are obtained from the other four compatibility relations. The resulting three equations may be solved for u_8, v_8, and w_8.

The noncharacteristic relation, Eq. (11), becomes

$$P_8 + \tfrac{1}{2}(\rho a^2)_8[u_x(8) + v_r(8) + w_\theta(8)/r_8]\Delta t = C_7 \tag{20}$$

$$C_7 = P_7 - \{\tfrac{1}{2}(\rho a^2)_7[u_x(7) + v_r(7) + w_\theta(7)/r_7] + (\rho a^2 v/r)_{78}\}\Delta t \tag{21}$$

The cross derivatives are eliminated from Eq. (20) by subtracting Eqs. (15), (17), and the finite difference forms of the other four bicharacteristic compatibility relations from Eq. (20) multiplied by four. The result, which may be solved for P_8, is

$$2P_8 - [(\rho a)_{18} - (\rho a)_{48}]u_8 - [(\rho a)_{28} - (\rho a)_{58}]v_8 - [(\rho a)_{38} - (\rho a)_{68}]w_8 = C_1 + C_2 + C_3 + C_4 + C_5 + C_6 - 4C_7 \tag{22}$$

The procedure presented in the above discussion determines the flow properties at an interior point to second-order accuracy by an explicit predictor-corrector procedure. No iterations or internal loops are required. Consequently, the procedure can be vectorized for extremely rapid execution on vector machines. In the present investigation, the procedure was implemented on a Cyber 205.

Solid Boundary Point Unit Process

The boundary condition applicable at solid boundary points is that the velocity normal to the boundary is zero. Since the boundary condition must be satisfied, the procedure developed in the previous section for an interior point unit process must be modified.

Five bicharacteristics, the pathline, and the boundary condition are required in the numerical integration scheme. The most convenient five bicharacteristics are those corresponding to $\bar{n} = \pm\bar{t}$, $-\bar{n}_b$, and $\pm\bar{s}$ at the points of intersection of the bicharacteristics and the initial-data hypersurface. The unit vectors $\bar{t}$ and $\bar{s}$ are chosen such that $\bar{t}$ is perpendicular to $\bar{n}_b$ and in the xr plane and $\bar{s}$ is orthogonal to $\bar{t}$ and $\bar{n}_b$, where $\bar{n}_b$ is the unit vector normal to the boundary. Point 1 corresponds to $\bar{n} = \bar{t}$, point 3 to $\bar{n} = \bar{s}$, point 4 to $\bar{n} = -\bar{t}$, point 5 to $\bar{n} = -\bar{n}_b$, and point 6 to $\bar{n} = -\bar{s}$. Point 2 corresponds to $\bar{n} = \bar{n}_b$, which points out of the flowfield, and is physically meaningless. Thus, bicharacteristic 2-8 is discarded and replaced with the boundary condition.

The procedure developed in the previous section to determine the flow properties at an interior point can be applied, with modifications, to a solid boundary point. The procedure is more complicated than the interior point unit process since, for a solid boundary, the characteristic normal $\bar{n}$ has x, r, and θ components, whereas, for the interior point, $\bar{n}$ has only an x, r, or θ component.

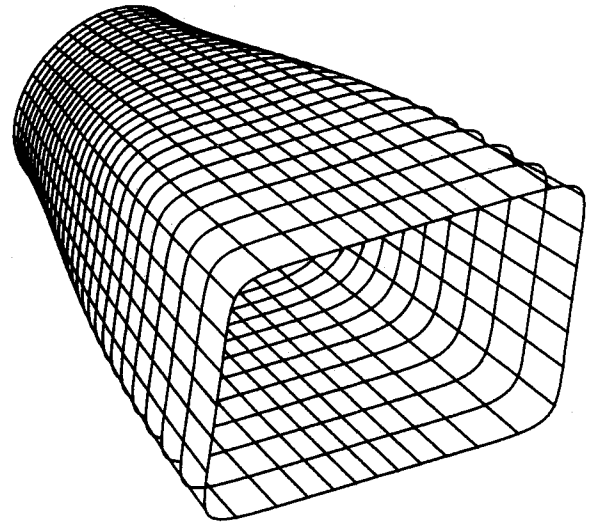

Fig. 6 Supersonic superelliptical nozzle.

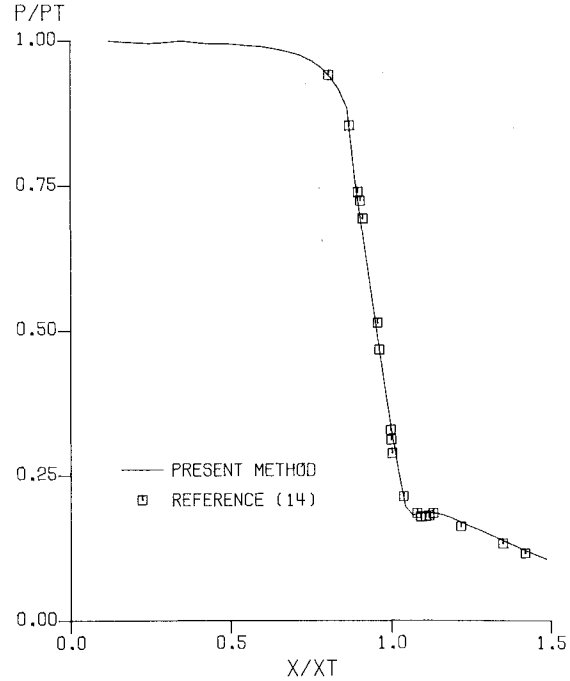

Fig. 5 Subsonic/transonic wall static pressure distribution.

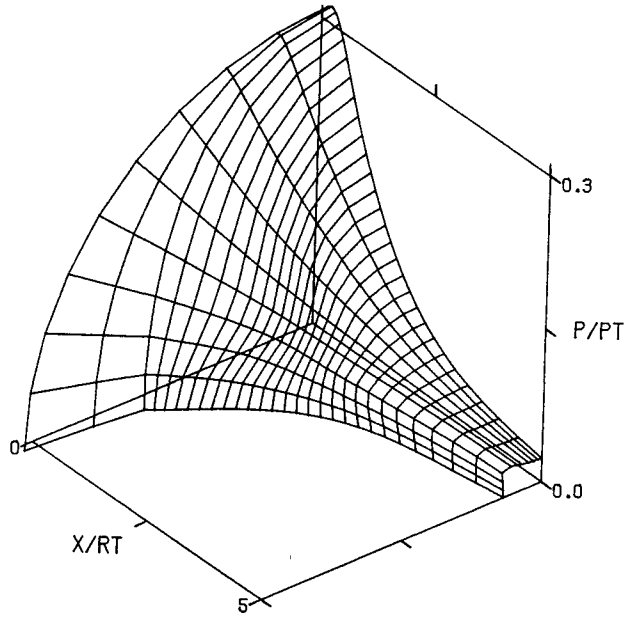

Fig. 7 Wall static pressure surface.

Inlet Point Unit Processes

Supersonic and subsonic inlet point unit processes are employed in the present method. The boundary conditions used at a supersonic inlet point are that the flow properties u, v, w, P, and ρ are all known and constant.

The boundary conditions used at a subsonic inlet point are that the stagnation pressure, stagnation temperature, and flow angles are known and constant. One bicharacteristic and the boundary conditions are required in the numerical integration scheme. The most convenient bicharacteristic corresponds to $\bar{n}=\bar{i}_x$.

For the predictor, the compatibility relation along bicharacteristic 1-8, Eq. (12), and the boundary conditions are solved for the flow properties u, v, w, P, and ρ at the solution point, point 8, using an iterative procedure, in which the Mach number is iterated. For the corrector, the same procedure is employed. A problem arises, however, with the evaluation of the cross derivatives at the solution point. They cannot be eliminated without using information at neighboring points in the solution hypersurface, so they are simply evaluated in the initial-data hypersurface. In the steady flow limit, the initial-data and solution hypersurfaces become identical, and second-order accuracy is achieved.

Supersonic Exit Point Unit Process

The supersonic exit point unit process is identical to the interior point unit process.

Axis Point Unit Process

The cylindrical coordinate system forms of the governing equations, Eqs. (1-5), are singular at an axis point ($r=0$). Consequently, the Cartesian coordinate system forms of the governing equations are employed at an axis point. A complete derivation of the characteristics equations for unsteady three-dimensional flow in Cartesian coordinates is presented by Hoffman.[8] The unit process for an axis point is similar to the unit process for an interior point.

Overall Numerical Algorithm

The overall solution at each time level is obtained by applying all of the previously discussed unit processes for a particular thermodynamic model, initial conditions, boundary conditions, and geometry.

The initial data, at time $t=0$, for the velocity magnitude, pressure, and density are obtained from a steady one-dimensional isentropic flow analysis. The initial values of the flow angles are obtained by linear interpolation along θ lines so that the flow at the centerline is in the x direction only and the flow at the wall is tangent to the wall and has x and r components only.

In the present investigation, the nozzle wall contour was specified by

$$[R_w(x,\theta)\cos\theta/R_a(x)]^{e(x)}+[R_w(x,\theta)\sin\theta/R_b(x)]^{e(x)}=1 \tag{23}$$

where $R_w(x,\theta)$ is the nozzle wall radius, $R_a(x)$ is the nozzle wall radius in the $\theta=0$ plane, $R_b(x)$ is the nozzle wall radius in the $\theta=\pi/2$ plane, and $e(x)$ is the superelliptical exponent. The nozzle cross sections can be circular, elliptical, or superelliptical. The cross section can change smoothly from one shape to another as a function of axial location.

The gas was assumed to be thermally and calorically perfect.

The time step between successive solution surfaces was determined by applying the Courant-Friedrichs-Lewy (CFL) stability criterion.[12] A stability analysis of the overall numerical algorithm was not attempted. Stability of the algorithm was demonstrated by actual numerical calculations.

Steady-state convergence was determined by marching in time in 500 time-step increments and inspecting the results. This process was repeated until the solution appeared to converge.

Both a scalar and a vector code were developed during the present study. The vector code was developed exclusively for the Cyber 205 computer. All of the code contained within the time-step loop was vectorized by use of "explicit" vector instructions.

Results

Results for several nozzle flowfields are presented to illustrate the capabilities of the computer program developed in the present investigation.

Supersonic Spherical Source Flow Study

A supersonic spherical source flow was analyzed to verify the computed results against a known exact solution. The source flow angle was 15 deg, the initial Mach number on the axis was 1.5, and the specific heat ratio was 1.4. Two different grids were analyzed. The coarsest grid had 15 axial locations and 7 radial locations (i.e., 15×7). The 29×13 grid had one-half the grid size of the 15×7 grid. The wall static pressure was found to be the most sensitive error indicator. Percent error in wall static pressure as a function of normalized axial position (normalized with the inlet radius) is presented in Fig. 2. The second-order accuracy of the numerical results is verified by comparison of the error for the two different grid sizes.

The algorithm was modified to employ MacCormack's method[9] at all interior points. Percent error in wall static pressure for the modified algorithm is presented in Fig. 2 for the 15×7 and 29×13 grids. Comparison of the results indicates that the error for the modified algorithm is comparable to, but slightly greater than, the error for the present method.

The supersonic spherical source flow errors for the present method were found to be comparable to, but slightly greater than, the errors for the steady two-dimensional supersonic flow direct-marching method of characteristics algorithm developed by Hoffman[13] and the steady three-dimensional

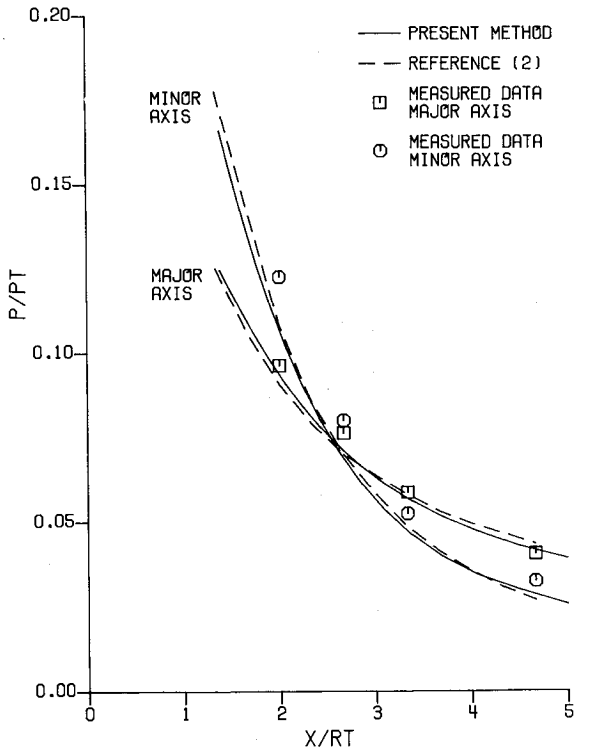

Fig. 8 Wall static pressure distributions.

supersonic flow inverse-marching method of characteristics algorithm developed by Ransom et al.[2]

Conical Nozzle Study

The subsonic/transonic/supersonic flowfield in the conical nozzle investigated experimentally by Cuffel et al.[14] was analyzed to verify the computed results against measured data. The geometry of the conical nozzle is illustrated in Fig. 3. The specific heat ratio was 1.4. Mach number contours in the transonic region are presented in Fig. 4. The measured data are the results obtained by Cuffel et al.[14] Good overall agreement is observed. The normalized wall static pressure (normalized with the nozzle inlet stagnation pressure) in the subsonic/transonic region as a function of normalized axial position (normalized with the axial location of the throat) is presented in Fig. 5. Good overall agreement is observed. The computed results presented in Figs. 4 and 5 were obtained with a 29×13 grid and correspond to 1000 time steps.

Supersonic Superelliptical Nozzle Study

The supersonic flowfield in the superelliptical nozzle investigated experimentally by Ransom et al.[2] was analyzed to verify the computed results against measured data. The geometry of the superelliptical nozzle is illustrated in Fig. 6. The throat radius is 0.75 in. and the throat radius of curvature is 0.75 in. The points of tangency between the circular arc throat and the parabolic nozzle wall contour for the major and minor axes are 16.5 and 7.0 deg, respectively. The axial distance from the throat to the nozzle exit is 3.75 in. The radii of the major and minor axes in the exit plane are 1.59 and 1.07 in., respectively. The wall slopes at the nozzle exit for the major and minor axes are 8.5 and 3.0 deg, respectively. The superelliptic exponent $e(x)$ [see Eq. (23)] varies from 2.0 at the throat to 10.0 at the exit. The specific heat ratio was 1.4.

An isometric view of the normalized wall static pressure surface (normalized with the nozzle inlet stagnation pressure) is presented in Fig. 7. The complex three-dimensional character of the flowfield is evident. Note that the highest pressure in the exit plane occurs in the corner, while the lowest pressure occurs at the minor axis. A prediction based on two-dimensional concepts would predict just the opposite result.

The normalized wall static pressure along the major and minor axes as a function of normalized axial position (normalized with the throat radius) is presented in Fig. 8 for two algorithms: 1) the present algorithm, and 2) the algorithm developed by Ransom et al.,[2] which determines the solution of steady three-dimensional supersonic nozzle

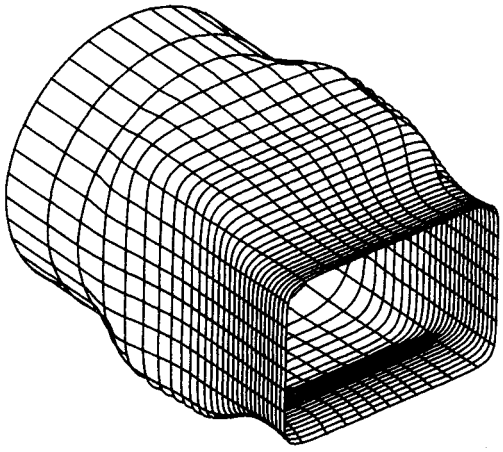

Fig. 9 Supersonic/transonic superelliptical nozzle.

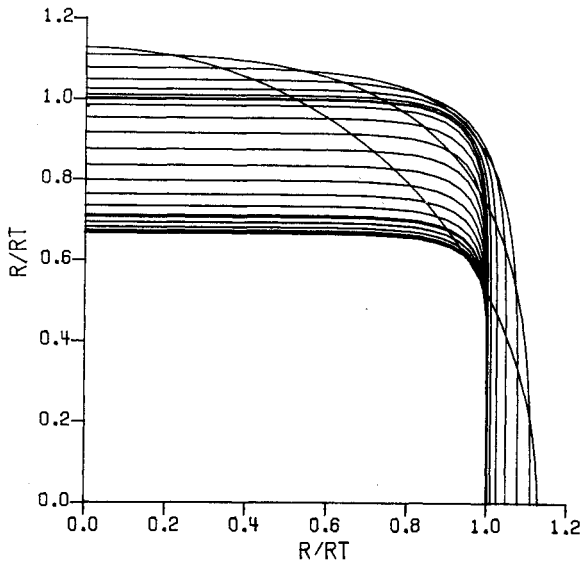

Fig. 10 Contour cross sections.

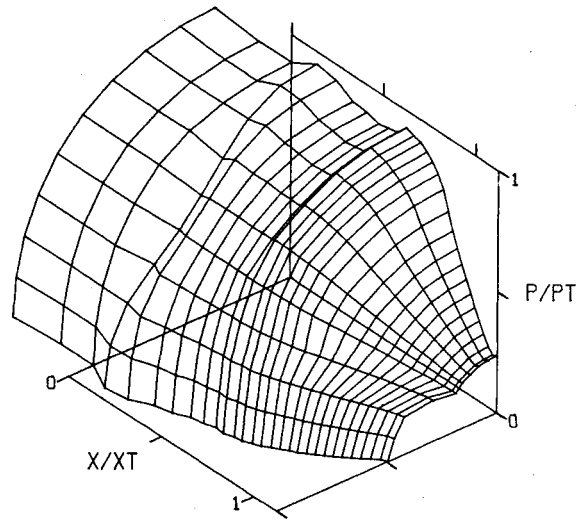

Fig. 11 Wall static pressure surface.

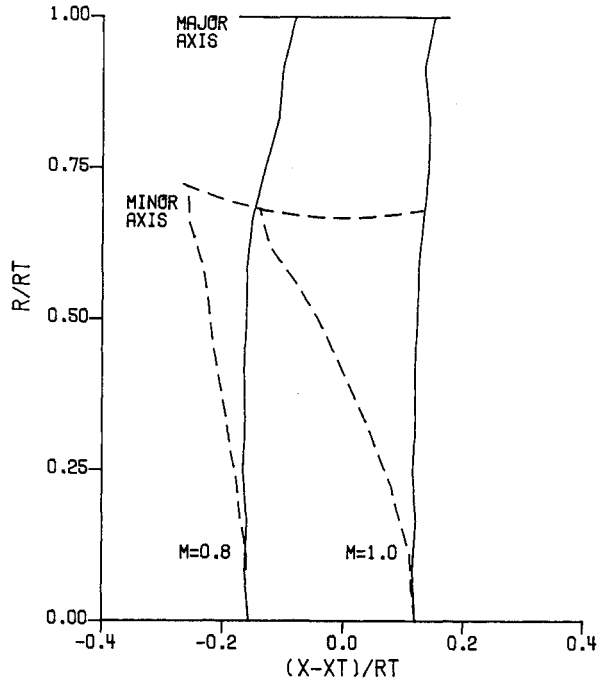

Fig. 12 Transonic Mach number contours.

Table 1 Computational speed

Code	Computer	Fortran compiler	Speed[a]
Present method scalar code	CDC 6500	Extended Version 4	55
Present method scalar code	CDC 6600	Extended Version 4	230
Present method scalar code	Cyber 205	Version 2.1	5,400
Present method vector code	Cyber 205	Version 2.1	21,000
MacCormack method scalar code	Cyber 205	Version 2.1	17,000
MacCormack method vector code	Cyber 205	Version 2.1	48,000

[a]Grid points calculated per second.

flows by Butler's method. The initial-value plane used by Ransom et al. was used as the inlet plane initial data in the present investigation. The measured data are the results obtained by Ransom et al. Good overall agreement between both the calculated results and the measured data is observed. The location where the pressure distributions along the major and minor axes intersect is correlated very well. The computed results presented in Figs. 7 and 8 were obtained with a $29\times13\times10$ grid and correspond to 2000 time steps.

Subsonic/Transonic Superelliptical Nozzle Study

The subsonic/transonic flowfield in the superelliptical nozzle illustrated in Fig. 9 was analyzed to demonstrate the unique capability of the present method to solve three-dimensional subsonic/transonic flows. The geometric parameters are normalized with the nozzle inlet radius. The axial distance from the inlet to the throat is 1.750, the throat radii for the major and minor axes are 0.886 and 0.591, respectively, and the throat radius of curvature for the minor axis is 0.591. The nozzle side walls along the major axis in the throat region are straight. The points of tangency between the circular arc throat and the parabolic nozzle wall contour for the minor axis, upstream and downstream of the throat, are 30 and 15 deg, respectively. The superelliptic exponent $e(x)$ [see Eq. (23)] varies from 2.0 at the inlet ($x=0$) to 10.0 at an axial distance from the inlet of 1.0. Cross sections of the nozzle at the axial computational locations, normalized by the major axis radius at the throat, are presented in Fig. 10.

Immediately downstream of the inlet, the cross-sectional area increases slightly. At an axial distance from the inlet of 1.0, the cross section is a square superellipse with a cross-sectional area approximately equal to the inlet area. The nozzle wall radius along the major axis is constant beyond an axial distance from the inlet of 1.0. A cylindrical section having a normalized length of 0.727 and containing two axial solution planes was added upstream of the nozzle inlet to allow the flow angle at the inlet to develop. The specific heat ratio was 1.3.

An isometric view of the normalized wall static pressure surface (normalized with the nozzle inlet stagnation pressure) is presented in Fig. 11. Note that the highest pressure in the exit plane occurs at the major axis and the lowest pressure occurs at the minor axis. A prediction based on two-dimensional concepts would predict just the opposite result.

Mach number contours for the major and minor axes are presented in Fig. 12. Note that for the minor axis the Mach number contours are similar to those for a conventional axisymmetric nozzle (see Fig. 4), whereas for the major axis the Mach number contours are nearly linear with a slight downstream tilt near the wall. The major axis Mach number contours cannot be explained by two-dimensional concepts.

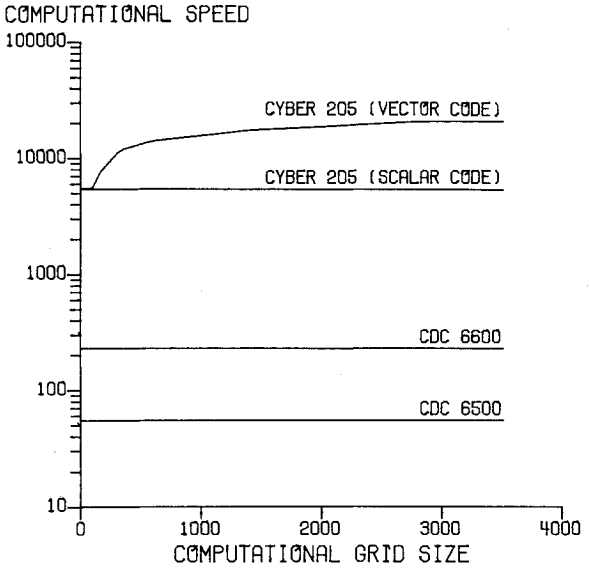

Fig. 13 Computational speed.

The computed results presented in Figs. 11 and 12 were obtained with a $29\times13\times10$ grid and correspond to 2500 time steps.

Computational Speed

A comparison of the computational speed (number of grid points calculated per second) for the computer program using the present method and MacCormack's method[9] at interior points is presented in Table 1. The Fortran Extended Version 4 and Version 2.1 compilers are multipass optimizing compilers. The computational speed results correspond to a $29\times13\times10$ grid. For the same number of grid points, the scalar code version of MacCormack's method is approximately three times faster than the scalar code version of the present method. For the same number of grid points, the vector code version of MacCormack's method is approximately two times faster than the vector code version of the present method.

Based on the limited error analysis in the source flow comparison presented earlier, some observations can be made. The error for MacCormack's method is roughly 1.5 times that for the present method. For equivalent errors, MacCormack's method would require approximately 1.8 times as many physical grid points as the present method, based on a second-order error comparison with a three-dimensional grid, and 1.2 times as many time steps to reach the same time. Thus, the computational speeds, modified to yield comparable accuracy, of MacCormack's method and the present method are approximately equal.

The computational speed of the present method is summarized in Fig. 13. The computational grid size (CGS) for an $IMAX\times JMAX\times KMAX$ grid is determined by

$$\mathrm{CGS}=(IMAX)(JMAX)(KMAX)-(IMAX)(KMAX-1)$$

where $IMAX$, $JMAX$, and $KMAX$ are the number of axial, radial, and angular grid locations, respectively.

Conclusions

A second-order accurate method of characteristics algorithm has been developed which is capable of analyzing a variety of three-dimensional subsonic/transonic flowfields. The execution time of the present method is comparable to that for fixed-grid finite difference algorithms. Solutions obtained by the present method agree well with solutions ob-

tained by the steady flow method of characteristics algorithms and experimental data. The high degree of accuracy, typical of method of characteristics algorithms, is retained in the present method, while the lengthy execution time usually associated with such algorithms has been eliminated. The result is a straightforward algorithm that can be easily programmed for both scalar and vector computers to yield a very efficient, accurate, robust, and versatile code.

Acknowledgments

This work was greatly enhanced by the invaluable assistance of Mr. David A. Seaman, User Services Programmer, Purdue University Computing Center, with vector programming on the Cyber 205. His efforts are sincerely appreciated.

References

[1]Butler, D. S., "The Numerical Solution of Hyperbolic Systems of Partial Differential Equations in Three Independent Variables," *Proceedings of the Royal Society of London*, Vol. 255A, 1960, pp. 232-252.

[2]Ransom, V. H., Hoffman, J. D., and Thompson, H. D., "A Second-Order Numerical Method of Characteristics for Three-Dimensional Supersonic Flow," *AIAA Journal*, Vol. 10, Dec. 1972, pp. 1573-1581.

[3]Cline, M. C. and Hoffman, J. D., "The Analysis of Non-equilibrium, Chemically Reacting, Supersonic Flow in Three-Dimensions Using a Bicharacteristics Method," *Journal of Computational Physics*, Vol. 12, May 1973, pp. 1-23.

[4]Vadyak, J., Hoffman, J. D., and Bishop, A. R., "Flow Computations in Inlets at Incidence Using a Shock Fitting Bicharacteristics Method," *AIAA Journal*, Vol. 18, Dec. 1980, pp. 1495-1502.

[5]Delaney, R. A. and Kavanagh, P., "Transonic Flow Analysis in Axial-Flow Turbomachinery Cascades by a Time-Dependent Method of Characteristics," *Journal of Engineering for Power*, July 1976, pp. 356-364.

[6]Shin, Y. W. and Valentin, R. A., "Numerical Analysis of Fluid-Hammer Waves by the Method of Characteristics," *Journal of Computational Physics*, Vol. 20, Feb. 1976, pp. 220-237.

[7]Marcum, D. L. and Hoffman, J. D., "Calculation of Unsteady Three-Dimensional Subsonic/Transonic Inviscid Flowfields by the Method of Characteristics," AIAA Paper 84-0440, Jan. 1984.

[8]Hoffman, J. D., "The Method of Characteristics Applied to Unsteady One-, Two-, and Three-Dimensional Flows," Thermal Sciences and Propulsion Center, School of Mechanical Engineering, Purdue University, West Lafayette, Ind., Rept. TR-80-07, June 1980.

[9]MacCormack, R. W., "The Effect of Viscosity in Hypervelocity Impact Cratering," AIAA Paper 69-354, April 1969.

[10]Zucrow, M. J. and Hoffman, J. D., *Gas Dynamics*, Vols. 1 and 2, John Wiley, New York, 1975.

[11]Rusanov, V. V., "The Characteristics of General Equations of Gas Dynamics," *Zhurnal Vychislitelnoi Mathematiki Mathematicheskoi Fiziki*, Vol. 3, 1963, pp. 508-527. Translated by K. N. Trirogoff, Literature Research Group, Aerospace Library Services, Aerospace Corp., San Bernardino, Calif., Rept. LRG-65-T-38, Oct. 1965.

[12]Courant, R., Friedrichs, K. O., and Lewy, H., "Uber die Partiellen Differenzialgleichungen der Mathematischen Physik," *Mathematische Annalen*, Vol. 100, 1928, pp. 32-74.

[13]Hoffman, J. D., "Accuracy Studies of the Numerical Method of Characteristics for Axisymmetric, Steady Supersonic Flows," *Journal of Computational Physics*, Vol. 11, Feb. 1973, pp. 210-239.

[14]Cuffel, R. F., Back, L. H., and Massier, P. F., "Transonic Flowfield in a Supersonic Nozzle with Small Throat Radius of Curvature," *AIAA Journal*, Vol. 7, July 1969, pp. 1364-1366.